

Magnetic Phase Diagram of FeAs based superconductors

Zhicheng Zhong, Qinfang Zhang, P. X. Xu and Paul J. Kelly
Faculty of Science and Technology and MESA⁺ Institute for Nanotechnology,
University of Twente, P.O. Box 217, 7500 AE Enschede, The Netherlands
(Dated: October 24, 2018)

The recently discovered high-temperature superconductivity in doped quaternary iron oxy-pnictides correlates experimentally with a magnetic instability. We have used first-principles calculations to determine a magnetic phase diagram of $\text{ReO}_{1-\delta}\text{FeAs}$ ($\text{Re}=\text{La-Dy}$) as a function of the doping δ , of the FeAs in-plane lattice constant a , and of the distance between the Fe and As planes, that is qualitatively consistent with recent experimental findings on the doping, internal (chemical) and external pressure dependence. The existence of a tricritical point (TCP) in the phase diagram suggests new ways of enhancing T_c .

PACS numbers:

The recent discovery of superconductivity in electron-doped $\text{La}[\text{O}_{1-x}\text{F}_x]\text{FeAs}$ with a critical temperature (T_c) of 26 K [1] has stimulated a massive experimental [2, 3, 4, 5, 6, 7, 8, 9, 10, 11, 12, 13, 14, 15] and theoretical effort [16, 17, 18, 19, 20, 21, 22, 23, 24, 25, 26, 27, 28] to find other, higher T_c materials in this completely new family of iron-pnictide superconductors. The undoped parent compound LaOFeAs is a poor metal with an ordered antiferromagnetic (AFM) ground state [5, 11] but with increasing F doping [12] the magnetic ordering is suppressed and superconductivity emerges. This strongly suggests that magnetic fluctuations in the iron layers close to the quantum critical point (QCP) play a fundamental role in the superconducting pairing mechanism. Recent experimental [12, 13, 14, 29] and theoretical [25, 26, 27, 28] results also suggest that spin fluctuations in the vicinity of the QCP mediate the superconductivity as in the cuprates, heavy fermion materials, or ruthenates [30, 31, 32]. In view of this, so far empirical, correlation between superconductivity and QCPs, it is important to understand how the magnetic (in)stability depends on structural and chemical parameters that are accessible to experiment. That is the subject of this paper.

Superconducting ReOFeAs crystallizes in a tetragonal layered structure with $P4/nmm$ symmetry and consists of layers of covalently bonded FeAs alternating with layers of more ionically bonded ReO. With eight atoms (two formula units) in the unit cell, it can be described using only two internal structural parameters in addition to the lattice parameters a and c [33]. One of the internal parameters, $d_{\text{Fe-As}}$, describes the separation between planes of Fe and As; the other, $d_{\text{Re-O}}$, between planes of Re and O. The excess electron from the ReO layer is donated to the FeAs layer which is metallic with a number of partly filled bands of mainly Fe $3d$ character intersecting the Fermi energy [19, 34]. In addition to the four structural parameters, we define a doping δ in terms of deviations from this ideal stoichiometry per Fe atom. Electron and hole doping can be achieved, for example,

by partially replacing oxygen with fluorine [1] or trivalent La with divalent Sr [35].

Since mapping out the magnetic phase diagram in five dimensions is impossible, we need to identify a smaller number of key independent variables. Clearly the doping δ is one. Although the interaction between the ReO and FeAs layers is by no means negligible, it is widely accepted that the superconducting properties of ReOFeAs emerge from the FeAs layers. The main role of the ReO layers is to determine the lattice parameters [33] and to contribute doping electrons while the magnetism and superconductivity are associated with the “active” FeAs layers so we fix $d_{\text{Re-O}}$ and c at their calculated equilibrium values for undoped LaOFeAs . The in-plane lattice constant a and the separation between the Fe and As layers $d_{\text{Fe-As}}$ [21, 22, 23, 24] are the other two key parameters we identify to construct magnetic phase diagrams in the $(\delta, a = a_{eq}, d_{\text{Fe-As}})$ and $(\delta = 0.25, a, d_{\text{Fe-As}})$ planes of this parameter space. We do this by calculating the energy $E(\delta, a, d_{\text{Fe-As}})$ for non-magnetic (NM), checkerboard AFM (C-AFM) and stripe AFM (S-AFM) orderings, going considerably beyond existing attempts to determine the QCPs of FeAs-based materials as a function of doping or pressure [25, 28].

The total energy calculations are carried out within the framework of density functional theory (DFT) using a spin polarized generalized gradient approximation (SGGA) for the exchange-correlation potential (PW91 functional). The electronic ground state is calculated by solving the Kohn-Sham equations self-consistently with the projected augmented wave method (PAW) [36] and a cut off energy of 500 eV for the plane wave basis as implemented in the Vienna *ab initio* simulation package (VASP) [37]. The C-AFM and S-AFM states are described in a $\sqrt{2} \times \sqrt{2} \times 1$ tetragonal structure. Though an orthorhombic distortion is observed [5, 21] for the S-AFM ordered state in the LaFeAsO parent compounds, it is suppressed by doping. Since we are mainly interested in locating the phase boundaries, it can be neglected. The Brillouin zone integrations are performed with the

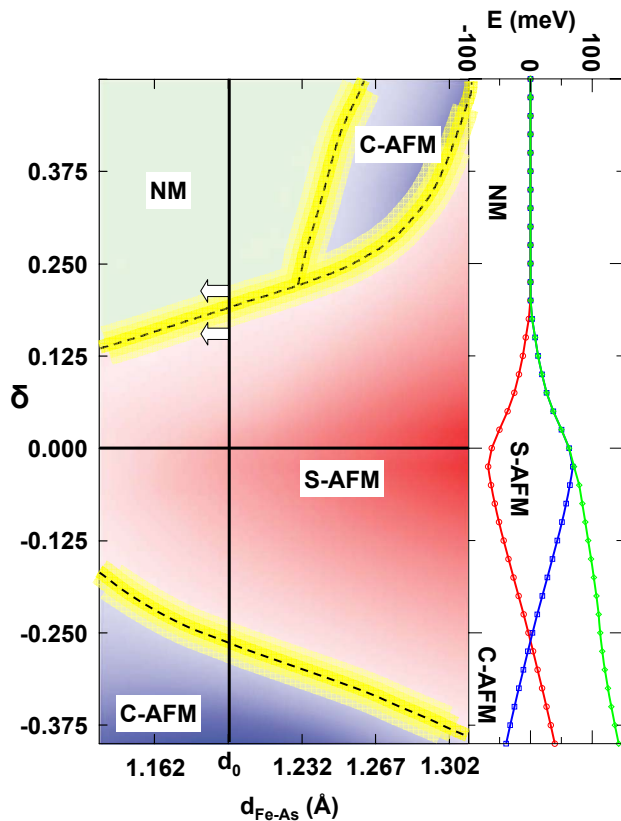


FIG. 1: Phase diagram of LaOFeAs as a function of doping δ and the distance between the Fe and As planes along the c axis, $d_{\text{Fe-As}}$. Blue, red and green represent respectively checkerboard AFM (C-AFM), stripe AFM (S-AFM) and non-magnetic (NM) ordering. In the AFM region, more stable magnetic ordering is described by darker color. d_0 is the calculated equilibrium value of $d_{\text{Fe-As}}$ for the undoped material. On the right hand side we show the energies per Fe atom of C-AFM, S-AFM and NM ordered states relative to their average value as a function of doping for the vertical line $d_{\text{Fe-As}} = d_0$. The white arrows describe the pressure dependence of over- and under-doped LaOFeAs.

improved tetrahedron method [38] with a sampling grid of $6 \times 6 \times 4$ k-points plus Γ point. When using pseudopotentials, it has been shown that it is necessary to treat the $3p$ states of Fe as valence states to reproduce all-electron results [24]. Doping was modelled by adding or subtracting electrons and compensating their charges with a homogeneous fixed background charge [37]. This approximation was checked explicitly using supercell calculations in which a fraction of the oxygen atoms were replaced with fluorine, and proved not to be critical.

We begin by determining the ground state of LaOFeAs as a function of δ and $d_{\text{Fe-As}}$. First of all the energy is minimized with respect to the internal structural parameters $d_{\text{Fe-As}}$ and $d_{\text{Re-O}}$ for the undoped parent compound LaOFeAs using the experimental a and c [39]. This optimized structure is then frozen and the total energy calculated as a function of $d_{\text{Fe-As}}$ and δ for NM, C-AFM

and S-AFM ordering. The phase diagram obtained from these energies is shown in Fig. 1 where positive and negative δ correspond to electron and hole doping, respectively. We propose that this phase diagram describes qualitatively all FeAs based materials since substituting different elements in the Re-O layers only changes the effective doping δ and the lattice parameters a and c . The effect of changing c , for example by external uniaxial pressure, is given in our phase diagram in terms of its effect on $d_{\text{Fe-As}}$; changing the Re position has otherwise little effect. The effect of changing a will be discussed below. Because our phase diagram is calculated as a function of two variables, the boundaries separating regions with different ground states, shown as dashed lines in Fig. 1, are in general quantum critical *lines* (QCL). The uncertainty in the location of these quantum critical lines resulting from neglecting the effect of differential relaxation specific to the magnetic ordering and doping, and because the SGGA is not exact, is indicated by the broader yellow regions.

The most notable feature of Fig. 1 is the asymmetry of electron and hole doping. The undoped material exhibits S-AFM ordering for all values of $d_{\text{Fe-As}}$ (horizontal line, $\delta = 0$) and S-AFM ordering is stabilized by increasing $d_{\text{Fe-As}}$. On doping LaOFeAs with electrons (vertical line, $d = d_0$), the S-AFM ordering is weakened and a transition to NM ordering is observed at $\delta \sim 0.18$. The suppression of magnetic ordering by electron doping is consistent with previous first-principles calculations [25, 40]. We can use this phase diagram to explain the dependence of T_c on external pressure. Experimentally it has been found that T_c increases with external pressure for $x < 0.14$ and decreases for $x > 0.14$ for $\text{Sm}[\text{O}_{1-x}\text{F}_x]\text{FeAs}$ [15]. This behavior indicates the existence of a QCP around $x \sim 0.14$. According to Fig. 1 the over-doped arsenide does not order magnetically while the under-doped ($x < 0.14$) material favours S-AFM order. External pressure will reduce $d_{\text{Fe-As}}$ (white arrows) but its effect on T_c depends on the doping. For under-doped $\text{Sm}[\text{O}_{1-x}\text{F}_x]\text{FeAs}$ it destabilizes the S-AFM ordering and pushes the system towards the QCL making it more susceptible to spin fluctuations. In agreement with observations [15], we expect this to enhance T_c . However, the over-doped system is NM and pressure drives it away from the QCL leading to lower values of T_c , as observed. When the structure is doped with holes, a transition to C-AFM ordering occurs. We will discuss below how the asymmetry of hole and electron doping can be understood in terms of the density of states (DOS) of the parent compound close to the Fermi level. Our phase diagram makes a clear prediction for the pressure dependence of T_c of hole doped iron arsenides, namely that it should be precisely the same as the electron-doped case electron-doped case.

A second notable feature of Fig. 1 is the existence of a narrow region between NM and S-AFM states where the

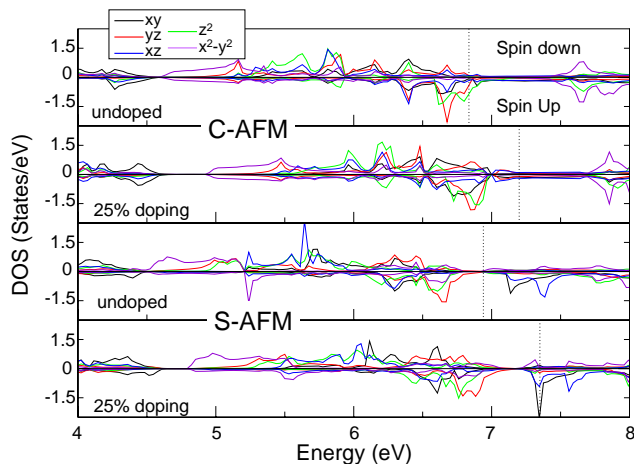


FIG. 2: Projected densities of states calculated for C-AFM ordered undoped and 25%-doped LaOFeAs; for S-AFM Fe ordered undoped and 25%-doped LaOFeAs. The orbital characters are color-coded. The Fermi energy is shown by the vertical dotted line.

ground state is C-AFM for large $d_{\text{Fe-As}}$ and high electron doping. The line separating NM and C-AFM states meets the line separating C-AFM and S-AFM states for an electron doping of $\delta \simeq 22\%$ and $d_{\text{Fe-As}} \simeq 1.03d_0$ in a tricritical point (TCP) where NM, S-AFM, and C-AFM states coexist. For electron doping $\delta > 22\%$, increasing $d_{\text{Fe-As}}$ generates a sequence of NM \rightarrow C-AFM \rightarrow S-AFM groundstates. To understand why this C-AFM region exists, we examine the Fe projected DOS shown in Fig. 2 for C-AFM and S-AFM ordering for undoped and 25% electron doping. For S-AFM ordering, the Fermi energy in the undoped case is situated in a pseudogap for both spin channels. On doping with electrons, the pseudogap has to be crossed before a high density of (mainly minority-spin) states peak with d_{xy} and $d_{x^2-y^2}$ character can be populated. This is energetically unfavourable. For C-AFM ordering, no such pseudogap exists and the doping electrons can be accommodated in states close to the undoped Fermi level while the large value of $d_{\text{Fe-As}}$ stabilizes the AFM states. It is the competition between these two mechanisms that results in the existence of a narrow region of C-AFM state.

In the context of heavy fermion and cuprate superconductivity, it has been suggested that spin fluctuations close to QCPs can give rise to the attractive interaction between carriers needed to mediate superconductivity [30, 31, 32]. The coexistence of NM, C-AFM, and S-AFM states at the TCP ($\delta \simeq 22\%$; $d_{\text{Fe-As}} \simeq 1.03d_0$) suggests that spin fluctuations there may be stronger and more interesting. We therefore propose searching for higher values of T_c in the vicinity of the TCP. This requires simultaneous achievement of large electron doping and negative pressures by suitable chemical substitutions.

Chemical pressure can be exerted by replacing La with

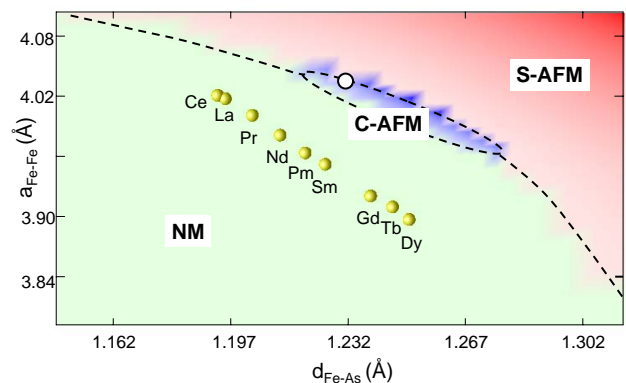


FIG. 3: Phase diagram of La[O_{0.75}F_{0.25}]FeAs as a function of lattice parameter a and inter-layer distance between Fe and As plane along c axis ($d_{\text{Fe-As}}$). The structure parameters obtained by geometry optimization for 25% doped Re compounds are plotted as yellow spheres. The color coding is the same as in Fig. 1. The white circle indicates the position of the tricritical point for a doping of $\delta = 0.22$.

other rare earth atoms, the in-plane lattice constant a and unit cell volume decreasing monotonically with decreasing Re size in the sequence La, Ce, Pr, Nd, Sm, Gd [33]. The effect of these substitutions has been studied experimentally resulting in the observation of a maximum value of $T_c = 55\text{K}$ for SmOFeAs [7, 8, 9, 10]. These substitutions change not only the lattice constants but also the internal parameter $d_{\text{Fe-As}}$. To study how sensitively the QCPs depend on a , we construct a phase diagram in the ($\delta = 0.25$, a , $d_{\text{Fe-As}}$) plane, Fig. 3. To achieve this high electron doping, we replace one out of four O atoms by a F atom in a $\sqrt{2} \times \sqrt{2} \times 1$ supercell in order to be able to more accurately describe distortions induced by the high concentration of the smaller F ion. The results agree well with those obtained on doping with the jellium model used to construct Fig. 1.

The main features of this phase diagram are (i) that the effect of increasing a is similar to that of increasing $d_{\text{Fe-As}}$: it stabilizes AFM ordering, and (ii) that the values of these structure parameters are not optimal. A small C-AFM “island” appears at the boundary between the NM and S-AFM “seas” in Fig. 3, consistent with Fig. 1. This C-AFM island represents an area where spin fluctuations are expected to be large. For a doping $\delta \sim 0.22$ corresponding to the TCP, this island shrinks to a point located at $d_{\text{Fe-As}} = 1.23\text{Å}$, $a = 4.04\text{Å}$, indicated in the figure by the white circle. We optimize the geometries of Re[O_{0.75}F_{0.25}]FeAs for Re = Ce, Pr, Nd, Pm, Sm, Gd, Tb, and Dy by energy minimization and plot the resulting structure parameters as yellow spheres in the figure [41]. Assuming that T_c is proportional to proximity to the TCP, we see that the Nd, Pm and Sm compounds should have the highest T_c s in agreement with observation [7]. The experimental data for ReO_{1- δ} FeAs (Re=La, Ce, Pr, Nd, Sm) [8] have been interpreted as

evidence for a lattice contraction induced enhancement of T_c . We note that replacing La with heavier Re elements is accompanied not only by a reduction of a but also by an increase in $d_{\text{Fe-As}}$. From the phase diagram of Fig. 1, we attribute the higher T_c primarily to the increase in $d_{\text{Fe-As}}$. We expect that the highest T_c will occur for doped NdOFeAs and SmOFeAs and that replacing Nd or Sm with heavier Re elements [10] will not lead to further improvement.

The phase diagram of Fig. 1 suggests that the optimal electron doping for FeAs based superconductors is around 22%. Electron doping can be reasonably well controlled experimentally by replacing O with F or by introducing oxygen vacancies. However Figs. 1 and 3 together indicate that currently achieved values of a and $d_{\text{Fe-As}}$ are smaller than the optimal values and should be increased to achieve higher values of T_c . One way of doing this would be to replace some As with the larger isovalent elements Sb or Bi or with Te.

In conclusion, we propose that the electronic structures and magnetic properties of FeAs-based superconductors such as LaOFeAs, BaFe₂As₂ and LiFeAs are dominated by the effective doping and structural details of the FeAs layers. In a QCP scenario, the superconductivity is related to spin fluctuations making it important to understand the magnetic phase diagram as a function of experimentally accessible parameters. Currently available experimental data can be understood using the theoretically obtained phase diagrams we have presented giving us confidence that they can then be used to search for higher values of T_c .

Acknowledgments: This work is part of the research program of the “Stichting voor Fundamenteel Onderzoek der Materie” (FOM) and the use of supercomputer facilities was sponsored by the “Stichting Nationale Computer Faciliteiten” (NCF), both financially supported by the “Nederlandse Organisatie voor Wetenschappelijk Onderzoek” (NWO). It is also supported by EC Contract No. IST-033749 DynaMax. The authors wish to thank S. Kumar and G. Brocks for useful discussions.

-
- [1] Y. Kamihara, T. Watanabe, M. Hirano, and H. Hosono, *Journal of the American Chemical Society* **130**, 3296 (2008).
- [2] H. Takahashi, K. Igawa, K. Arii, Y. Kamihara, M. Hirano, and H. Hosono, *Nature* **453**, 376 (2008).
- [3] F. Hunte, J. Jaroszynski, A. Gurevich, D. C. Larbalestier, R. Jin, A. S. Sefat, M. A. McGuire, B. C. Sales, D. K. Christen, and D. Mandrus, *Nature* **453**, 903 (2008).
- [4] X. H. Chen, T. Wu, G. Wu, R. H. Liu, H. Chen, and D. F. Fang, *Nature* **453**, 761 (2008).
- [5] C. de la Cruz, Q. Huang, J. W. Lynn, J. Li, W. Ratcliff II, J. L. Zarestky, H. A. Mook, G. F. Chen, J. L. Luo, N. L. Wang, et al., *Nature* **453**, 899 (2008).
- [6] G. F. Chen, Z. Li, D. Wu, G. Li, W. Z. Hu, J. Dong, P. Zheng, J. L. Luo, and N. L. Wang, *Phys. Rev. Lett.* **100**, 247002 (2008).
- [7] Z.-A. Ren, W. Lu, J. Yang, W. Yi, X.-L. Shen, Z.-C. Li, G.-C. Che, X.-L. Dong, L.-L. Sun, F. Zhou, et al., *CHIN. PHYS. LETT.* **25**, 2215 (2008).
- [8] Z.-A. Ren, G.-C. Che, X.-L. Dong, J. Yang, W. Lu, W. Yi, X.-L. Shen, Z.-C. Li, L.-L. Sun, F. Zhou, et al., *Europhys. Lett.* **83**, 17002 (2008).
- [9] Z.-A. Ren, J. Yang, W. Lu, W. Yi, X.-L. Shen, Z.-C. Li, G.-C. Che, X.-L. Dong, L.-L. Sun, F. Zhou, et al., *Europhys. Lett.* **82**, 57002 (2008).
- [10] J.-W. G. Bos, G. B. S. Penny, J. A. Rodgers, D. A. Sokolov, A. D. Huxleyac, and J. P. Attfield, *Chem. Commun.* **2008**, 3634 (2008).
- [11] J. Dong, H. J. Zhang, G. Xu, Z. Li, G. Li, W. Z. Hu, D. Wu, G. F. Chen, X. Dai, J. L. Luo, et al., *Europhys. Lett.* **83**, 27006 (2008).
- [12] Y. Nakai, K. Ishida, Y. Kamihara, M. Hirano, and H. Hosono, *J. Phys. Soc. Jpn.* **77**, 073701 (2008).
- [13] Y. Kohama, Y. Kamihara, M. Hirano, H. Kawaji, T. Atake, and H. Hosono, *Phys. Rev. B* **78**, 020512(R) (2008).
- [14] A. J. Drew, F. L. Pratt, T. Lancaster, S. J. Blundell, P. J. Baker, R. H. Liu, G. Wu, X. H. Chen, I. Watanabe, V. K. Malik, et al., *Phys. Rev. Lett.* **101**, 097010 (2008).
- [15] Y. Takabayashi, M. T. McDonald, D. Papanikolaou, S. Margadonna, G. Wu, R. H. Liu, X. H. Chen, and K. Prassides, *Journal of the American Chemical Society* **130**, 9242 (2008).
- [16] K. Haule, J. H. Shim, and G. Kotliar, *Phys. Rev. Lett.* **100**, 226402 (2008).
- [17] C. Cao, P. J. Hirschfeld, and H.-P. Cheng, *Phys. Rev. B* **77**, 220506(R) (2008).
- [18] F. Ma and Z.-Y. Lu, *Phys. Rev. B* **78**, 033111 (2008).
- [19] D. J. Singh and M.-H. Du, *Phys. Rev. Lett.* **100**, 237003 (2008).
- [20] L. Boeri, O. Dolgov, and A. A. Golubov, *Phys. Rev. Lett.* **101**, 026403 (2008).
- [21] T. Yildirim, *Phys. Rev. Lett.* **101**, 057010 (2008).
- [22] Z. P. Yin, S. Lebegue, M. J. Han, B. P. Neal, S. Y. Savrasov, and W. E. Pickett, *Phys. Rev. Lett.* **101**, 047001 (2008).
- [23] S. Ishibashi, K. Terakura, and H. Hosono, *J. Phys. Soc. Jpn.* **77**, 053709 (2008).
- [24] I. I. Mazin, M. D. Johannes, L. Boeri, K. Koepernik, and D. J. Singh, *Phys. Rev. B* **78**, 085104 (2008).
- [25] G. Giovannetti, S. Kumar, and J. van den Brink, *Physica B* **403**, 3653 (2008).
- [26] I. I. Mazin, D. J. Singh, M. D. Johannes, and M. H. Du, *Phys. Rev. Lett.* **101**, 057003 (2008).
- [27] K. Kuroki, S. Onari, R. Arita, H. Usui, Y. Tanaka, H. Kontani, and H. Aoki, *Phys. Rev. Lett.* **101**, 087004 (2008).
- [28] G. Xu, H. Zhang, X. Dai, and Z. Fang, *cond-mat/* pp. 0807.1401– (2008).
- [29] R. H. Liu, G. Wu, T. Wu, D. F. Fang, H. Chen, S. Y. Li, K. Liu, Y. L. Xie, X. F. Wang, R. L. Yang, et al., *Phys. Rev. Lett.* **101**, 087001 (2008).
- [30] N. D. Mathur, F. M. Grosche, S. R. Julian, I. R. Walker, D. M. Freye, R. K. W. Haselwimmer, and G. G. Lonzarich, *Nature* **394**, 39 (1998).
- [31] T. Moriya and K. Ueda, *Rep. Prog. Phys.* **66**, 1299 (2003).
- [32] P. Monthoux, D. Pines, and G. G. Lonzarich, *Science*

- 450**, 1177 (2007).
- [33] P. Quebe, L. J. Terbüchte, and W. Jeitschko, *J. Alloys Compd.* **302**, 70 (2000).
- [34] S. Lebègue, *Phys. Rev. B* **75**, 035110 (2007).
- [35] H.-H. Wen, G. Mu, L. Fang, H. Yang, and X. Zhu, *Europhys. Lett.* **82**, 17009 (2008).
- [36] P. E. Blöchl, *Phys. Rev. B* **50**, 17953 (1994).
- [37] G. Kresse and J. Furthmüller, *Phys. Rev. B* **54**, 11169 (1996).
- [38] P. E. Blöchl, O. Jepsen, and O. K. Andersen, *Phys. Rev. B* **49**, 16223 (1994).
- [39] The calculated SGGA values of a and c are 0.402 and 0.863, very close to the experimental values of 0.404 and 0.875 nm, respectively [33].
- [40] G. Xu, H. Zhang, X. Dai, and Z. Fang, *cond-mat/ pp.* 0807.1401– (2008).
- [41] Pseudopotentials for the Re elements Ce-Dy with the 4f electrons treated as core electrons and for La are calculated in slightly different ways so that the calculated structure parameters are not strictly comparable.